CHARACTERIZATION OF MSD IN EMERGING METALLIC STRUCTURES IN FUSELAGE LAP JOINTS

Kevin Stonaker[1], John G. Bakuckas, Jr.[1], Terry Zhang[2], Mike Kulak[3], Kimberly Maciejewski[4], Walt Sippel[5], Fabricio Fanton[6], Carlos E. Chaves[6], and Paul Jonas[7]

[1] FAA William J. Hughes Technical Center, Atlantic City, NJ 08405, USA; kevin.stonaker@faa.gov
[2] Drexel University, Philadelphia, PA 19104, USA
[3] Diakon Solutions LLC, Cape May Court House, NJ, 08210, USA
[4]Arconic Technology Center, New Kensington, PA, 15068, USA
[5] FAA Transport Standards Branch, Des Moines, Washington 98198, USA
[6] Embraer, São José dos Campos, Brazil
[7] National Institute for Aviation Research, Wichita, KS, 67260, USA

In partnership with Arconic, Embraer, and the National Institute for Aviation Research (NIAR), the Federal Aviation Administration (FAA) is evaluating the behavior of multi-site damage (MSD) for emerging aluminum alloys in a generic fuselage lap joint configuration. This program is a comparative study of the initiation and growth characteristics of MSD for two aerospace aluminum alloys, namely 2524-T3 aluminum-copper alloy (baseline) and 2060-T8 aluminum-lithium alloy (new generation). This behavior is being studied by conducting fatigue testing on a common lap joint design at three different specimen sizes: (1) single rivet column coupons, (2) wide flat panel specimens, and (3) curved sub-scale panel specimens. Data from this study will be used to assess the relevance of existing regulations and to inform whether additional safety standards and regulatory guidance should be developed to provide improved safety beyond that afforded by the existing airworthiness standards. Additionally, results will be used to support potential improved weight and structural safety performance expectations of the emerging metallic structures technologies (EMST) and to evaluate the effect of specimen scale on fatigue performance.

As part of this program, a subset of the 2524-T3 wide flat panels and curved sub-scale panels were manufactured with an initial MSD scenario. The purpose of the MSD scenario was to establish a common starting point for the crack growth and residual strength portions of the tests to facilitate better post-test comparisons. Additionally, based on finite element modelling, it was anticipated that the wide flat panels would experience higher secondary bending of the joint compared to the curved sub-scale panels. Accordingly, a subset of the MSD wide flat panels were also tested in a constrained manner to bring it closer to the predicted curved panel behavior. This paper will provide a brief overview of this program with focus on the test and analysis of the wide flat and curved sub-scale panel with the initial MSD scenario. Results to date showed that for the specimens tested in this program the curved sub-scale panels generally had a shorter fatigue life compared to the wide flat panels and constraining the wide flat panels did reduce secondary bending but had a minimal effect on fatigue life. Work for this program is still ongoing so this paper represents results generated at time of print only.

Keywords: Multi-site damage, Lap joint, Fatigue, Emerging metallic structures technology

INTRODUCTION AND BACKGROUND

For decades, the aerospace industry has relied on incremental improvements in metallic materials for aircraft design and manufacturing. This reliance has changed significantly in recent history with the introduction of composite materials and other advanced manufacturing techniques. In response, the aluminum industry has made large strides to introduce new aluminum and aluminum-lithium alloys. In combination with advanced manufacturing innovations, these new alloys – which offer varying combinations of lower densities, higher strength, and improved damage tolerance – provide opportunities for competitive performance at lower build costs.

The Federal Aviation Administration (FAA), Arconic, Embraer, and the National Institute for Aviation Research (NIAR) have partnered to evaluate several emerging metallic structures technologies (EMST) through test and analyses [1-3]. The goal is to demonstrate the potential for fuselage concepts using EMST to improve durability and damage tolerance compared with the current baseline aluminum fuselage and to assess the relevance of existing damage-tolerance regulations and associated guidance materials. As part of this program, a study on the behavior of multi-site damage (MSD) in fuselage lap joint structure is being conducted. This work focuses on several aspects of lap joint behavior, including identifying if any unique damage modes or MSD behavior exist for new alloys, evaluating the influence of manufacturing parameters, evaluating the difference between coupon scales, and exploring the potential to compensate for coupon scale effects. The data gained will help substantiate widespread fatigue damage (WFD) test methodologies and the evaluation of supporting analytical methods.

The behavior of fuselage lap joints is a complex problem [4-6]. Multiple design aspects can play a large role in joint behavior including overlap length, fastener spacing, and fastener installation. In addition, manufacturing and assembly methods as well as laboratory testing considerations such as coupon size, coupon form (flat vs. curved), and loading method (uniaxial, biaxial, or pressurized) influence test results [6]. Adding to that, the natural variability in crack initiation and growth makes an exhaustive study of MSD behavior quite challenging.

This test program has been constructed to focus on several considerations mentioned above. The overall test program involves two materials, 2524-T3 and 2060-T8 Al-Li, and two rivet materials, 2117-T4 (AD) and 7050-T73 (E). It also uses a lap joint design that is used at three different coupon scales: single rivet column, wide flat panels, and curved sub-scale panels. The lap joint design is meant to represent a simplified single aisle longitudinal fuselage lap joint with three rivet rows. Specimens were all manufactured by the National Institute for Aviation Research (NIAR) in either the pristine condition for crack initiation studies or with an initial MSD scenario of electro discharge machined (EDM) notches for focused crack growth, interaction, and link-up studies. The work within this program is currently ongoing so this paper will focus only on the 2524-T3 MSD scenario panels at the wide flat and curved sub-scale coupon levels.

EXPERIMENTAL AND ANALYTICAL METHODS

The basis for the work presented in this paper is comparative tests between wide flat and curved sub-scale lap joints. A consistent joint design was used for all specimens to facilitate comparison between the different configurations tested. Additionally, all the results presented are for the 2524-T3 material specimens using MS14218AD5 rivets with an identical initial MSD notch scenario. The scenario used, Figure 1, represents a lead crack situation with smaller MSD cracks present at the surrounding rivet locations. Starting from this consistent damage scenario facilitates crack growth behavior comparisons

between all the specimens. In addition to the MSD notch scenario, the wide flat panels were tested in a constrained and unconstrained condition. The purpose of this constraint condition was to reduce joint secondary bending for a subset of flat panels in an attempt to match the bending of the curved sub-scale panels more closely. More detail on the reasoning and execution of this is provided in following sections. A look at the configuration sizes and test matrix represented in this paper are shown in Figure 2.

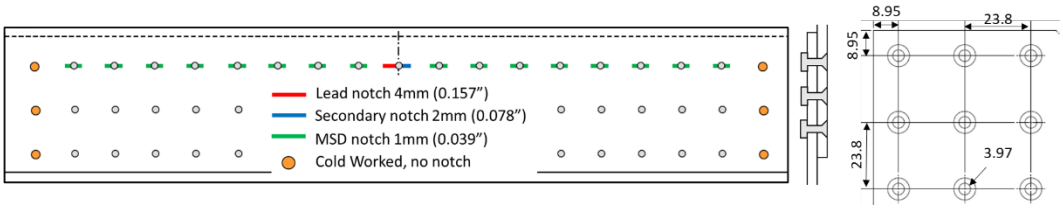

Figure 1. MSD Scenario and joint design (dimensions in mm)

Sheet Material	Thickness (mm)	Grain Orientation	Configuration	Rivet Type	Quantity		
					Wide Flat Panels		Curved Sub-scaled Panel
					Unconstrained	Constrained	
2524-T3	1.6	T-L	Notched MSD	MS14218AD5 (2117-T4)	2	2	3

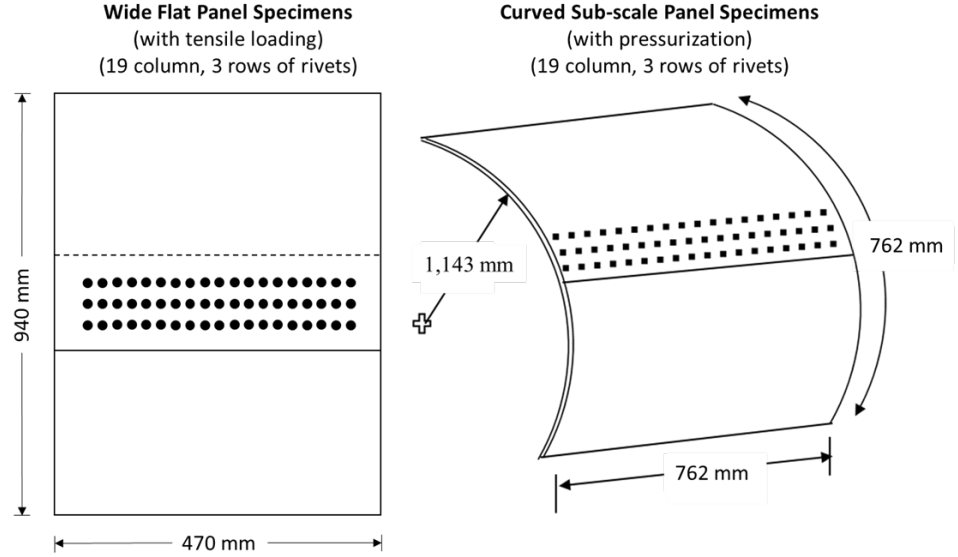

Figure 2: Test matrix and panel configurations.

Finite Element Analysis

As mentioned above, the behavior of a lap joint is very complex, so it is important to understand this behavior and be able to model it accurately. An integral part of this program is the analytical work being conducted by Embraer and Drexel University to support the physical testing. Finite element models (FEM) were created for each of the coupon sizes and configurations. They were used to quantify the expected differences between the coupons and were the basis for attempts to modify coupon behavior in the form of an anti-bending device installed on some wide flat panels.

One well known aspect of lap joint loading is the presence of secondary bending created by eccentricity in the joint load path. This bending can be a considerable driver in crack initiation and growth as it directly contributes to high stresses at critical points in the joint. While secondary bending is largely driven by lap joint design (i.e., number of rivet rows, row spacing, or material thickness), some of these effects are accounted for in this program by the common joint design. However, the loading mechanism for the wide flat and curved sub-scale panels is different. The flat panels are uniaxially loaded while the curved sub-scale panels are mounted in a test frame which constrains all sides and is internally pressurized. As the finite element model results show in Figure 3, this difference has a significant effect on the bending for the two different coupons. The wide flat panel is expected to have considerably more bending compared to the curved sub-scale panel. One goal of this work was to devise a way to control

the bending of the wide flat panel to bring it closer to that of the curved sub-scale panel as shown in Figure 3. This is the basis for the constrained wide flat panel tests that will be covered later in the test setup section.

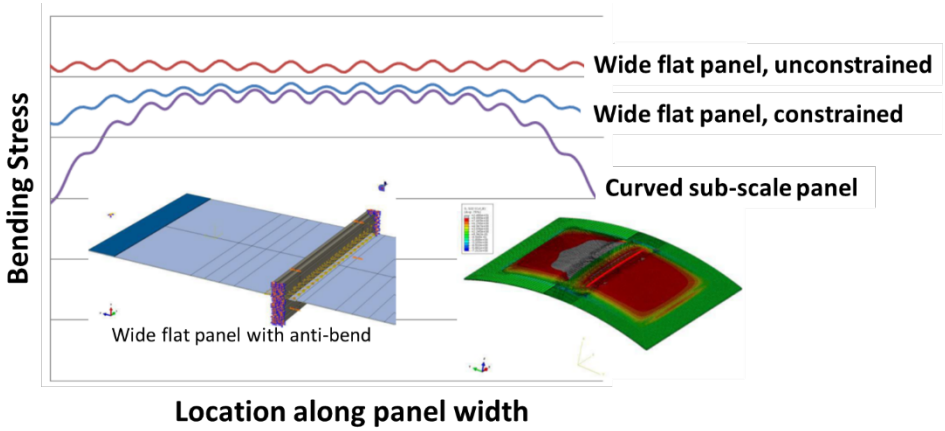

Figure 3: Finite element analysis of curved sub-scale and wide flat panels.

Stress Intensity Factor Solutions

To make a connection between the test and analysis portions of this work, two methods were used to calculate the stress intensity factor (SIF) at the crack tip for varying crack lengths. Both methods rely on strain field outputs from digital image correlation (DIC) taken in the area of the lead crack.

The first method, based on work by Dally and Sanford [7] is based on Westergaard's equation and uses the strain field in front of the crack tip along an angle to the crack direction. Selecting a strain path of 60 degrees relative to the current crack direction allows for the SIF to be calculated using the Westergaard solution. The SIF was measured early in the test to facilitate a direct comparison between all panels. This strategy avoids major differences between the panels in later stages of crack growth, including, differences in crack angle deviation, crack front geometry through the thickness, and distances between measured and adjacent cracks. Currently, this method assumes Mode I is the dominant mode but this approach will be expanded in the future to include all modes.

The second method uses the measured strain field around the crack tip to calculate the J integral. A series of sections cuts are made in the DIC software such that a strain contour around the crack tip is generated. A Matlab program was then built to take the section cuts and calculate the J integral for the given strain state. One advantage to the J integral approach is that the strain field measurements can be taken further from the crack tip compared to the crack tip strain field approach described above, because the J integral is path independent. However, for the current lap joint geometry, this advantage is limited by the small distance between the measured crack tip and approaching crack tip.

TEST SETUP

During service, the longitudinal fuselage lap joint is cyclically loaded by cabin pressurization. The curved sub-scale panels are mounted on all sides and pressurized in a similar manner. To be consistent, the flat panel tests were all conducted as constant amplitude tension-tension fatigue tests. The applied loads were selected to create a far field stress of 87.5 MPa. The R ratio for testing was 0.1. While the loading conditions and joint designs were made the same, different mounting approaches and loading mechanisms cannot be avoided. The internal pressurization of the curved sub-scale panels leads to a biaxial loading versus uniaxially mechanical loading for the wide flat panels.

Additionally, a marker band spectrum was implemented into the load history by systematically reducing the max load to 75% of fatigue for a set number of cycles in a predetermined pattern. This is shown schematically in Figure 4. The marker bands generally alternated between 7 and 3 patterns with a special

10 marker band pattern placed when the lead crack extension reached 1 mm for the wide flat panels. The marker band spectrum leaves distinct beach marks on the fracture surface that greatly simplifies post-test fractography [8,9].

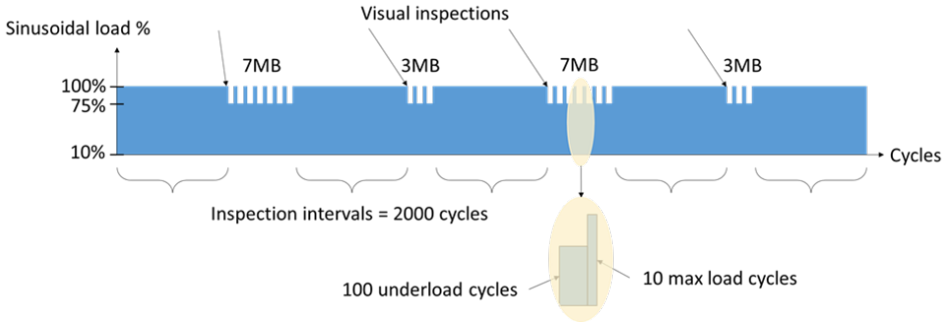

Figure 4: Marker band spectrum.

To facilitate comparison between the various aspects of the test program, it was important to maintain consistency for the different coupon scales. In addition to the consistent lap joint design mentioned above, all the coupons in this work use a single lot of 2524-T3 and were manufactured by NIAR using typical industry practices.

The fatigue test program is implemented in three distinct phases. The first phase is crack sharpening. As is typical with manufactured notches, there was an initial sharpening period needed for natural cracks to form. The sharpening was done at full scale fatigue load but those cycles were excluded in the results presented later. The second phase is short crack growth. This was defined as crack growth up to 1 mm of crack extension from the EDM notch for the lead crack. During this phase, inspections were conducted and marker bands placed every 1,000 cycles. Once the lead crack reached 1 mm of growth the first set of DIC images were taken. The final stage is defined as crack growth up to plastic zone link-up between the lead and adjacent MSD cracks. During this phase, inspections and marker bands were 2,000 cycles apart. Fatigue cycling ended once plastic zone link-up was reached. The wide flat panels did undergo residual strength tests following plastic zone link-up, but those results are not presented here due to paper length constraints. Those results will be published in a future FAA report.

The FAA William J. Hughes Technical Center and Embraer tested the wide flat panels and curved sub-scale panels, respectively. The inspection methods differed slightly between the two labs. Both used identical strain gage and DIC patterns. The FAA used phased array ultrasonic inspection during the sharpening and small crack growth phases. They also used a traveling optical microscope to record surface crack measurements throughout the test. Since the curved sub-scale panels tested by Embraer were internally pressurized, safety issues precluded visual inspection while under load. Instead, Embraer conducted high frequency eddy current inspection on the unpressurized panel. During the inspection periods, quasi-static strain surveys and DIC image collections were conducted up to full fatigue load and surface crack measurements were taken for both sides of all rivets with initial EDM notches.

Flat Panel Testing

The Technical Center was responsible for testing the wide flat panels. This was done on a uniaxial MTS load frame with a 245 kN (55 kip) load cell. Steel load plates were bolted to each end of the specimens and attached to the load frame at each end by a clevis. The wide flat panels also had spacing shims bonded to opposing end at the load attachment areas to prevent any fixture induced eccentricity. The tests were run under load control at a rate of up to 3 hertz.

The FAA also used an anti-bend device for half of the wide flat panel tests. As mentioned previously, this was done to reduce the secondary bending in an attempt to have the constrained flat panels behave more like the curved sub-scale panels, specifically near the critical rivet row with EDM notches. The anti-bend device, shown installed on a wide flat panel in Figure 5, was predominately constructed from commercial t-slotted aluminum bars. The concept for the design comes from the use of anti-buckling

supports for thin sheet crack growth tests. Here, two bars are placed opposite each other along the width of the panel at the central rivet with the t-slot giving clearance for the rivet heads. These cross bars are then connected to supporting bars that are anchored at the top steel load plate and floating at the lower steel load plate. Large steel c-clamps are also installed on the cross bars to give additional support as well as to control the force applied to the panel. Teflon tape was used between the cross bars and the panels to minimize tension load being transfer away from the panel and to the anti-bend device.

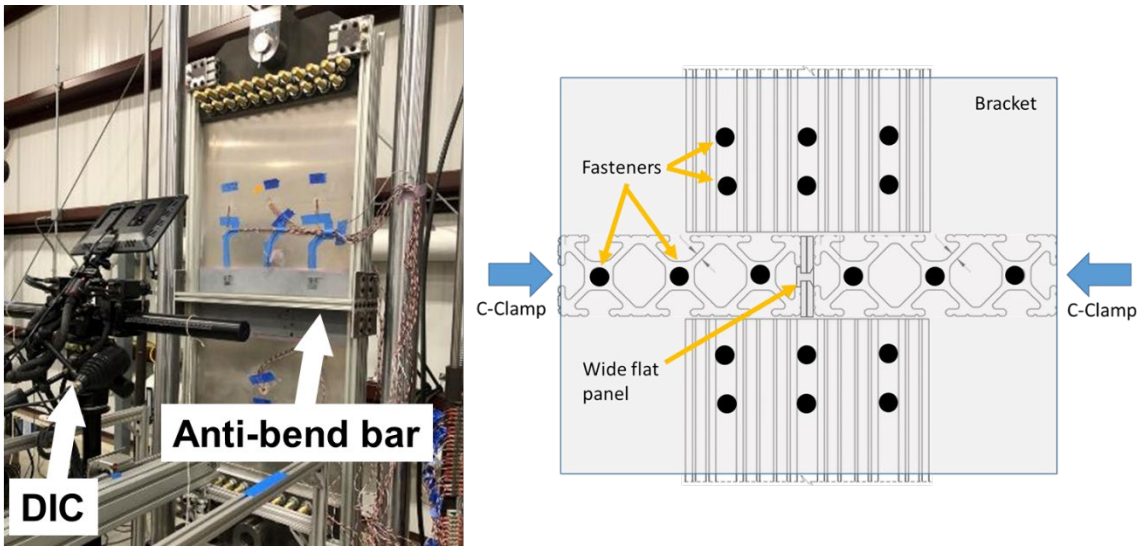

Figure 5: Wide flat panel test setup with anti-bend bar (constrained)

Curved Sub-scale Panel Testing

Embraer was responsible for testing the curved sub-scale panels. This was done on a customized fixture made to test curved panels under internal pressurization. The fixture, shown below in Figure 6, is designed to test panels with a radius of 1,143 mm. The panels are fixed on all four sides to the fixture and internally pressurized by air. The tests were run at a rate of approximately 0.5 hertz.

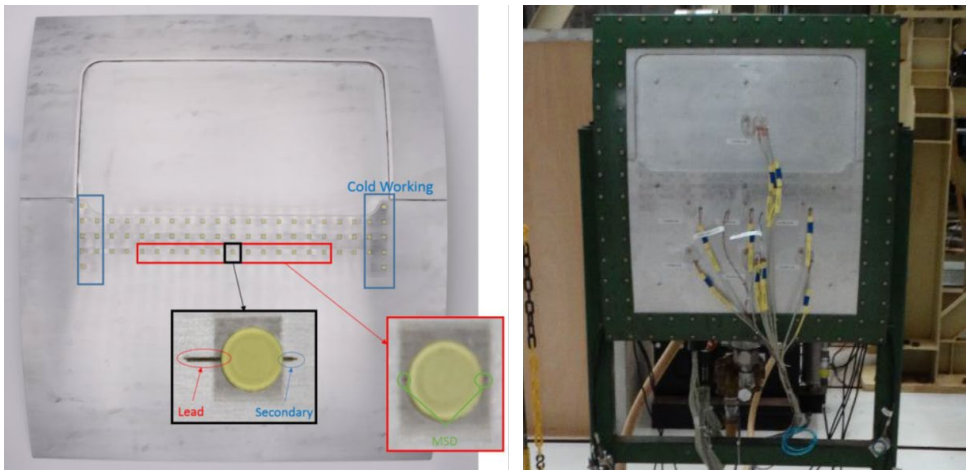

Figure 6: Curved Sub-scale Panel Test Setup

RESULTS

Anti-Bend Trial Results

The first phase of this program was to build and test the anti-bend device described above. The goal for the device was to constrain the secondary bending of the wide flat panel without otherwise affecting the general loading of the panel. FEA was used to show that the placement of the device around the center rivet row did not materially change the loading of the critical rivet row outside of the reduced bending.

A series of strain surveys were used to show that the anti-bend device was effective in its task. Both the wide flat and curved sub-scale panels all had three sets of front to back strain gage pairs installed just outside the joint area and a fourth pair installed in the center far-field region. Strain gages were also installed on the C-clamps used for the anti-bend device to enable controlled and repeatable application. The gage pairs allowed strain to be broken down to tension and bending components as shown in Eq. 1 and 2 respectively. Here ε_1 and ε_2 represent strain from the front and back strain gage pairs.

$$\varepsilon_{Tension} = \frac{1}{2} * |\varepsilon_1 + \varepsilon_2| \quad (1)$$

$$\varepsilon_{Bending} = \frac{1}{2} * |\varepsilon_1 - \varepsilon_2| \quad (2)$$

The series of strain surveys considered the unconstrained wide flat panel results as the baseline state. The anti-bend fixture was then tested in various states. First it was tested without the C-clamps and then with the C-clamps at different clamping forces. Finally, the curved sub-scale panel was also tested and served as the target for bending reduction. Figure 7 shows the change for various constrain conditions relative to the unconstrained condition for the wide flat panels only. The trials were successful in showing the anti-bend device could reduce the secondary bending without materially altering the tensile loads on the panel, ~30% reduction versus ~2% reduction respectively. The trials were also used to establish the desired clamping force of the C-clamps, Figure 8. Note that in Figure 8 the relatively large change in bending strain due to the anti-bend device is less significant when comparing to the larger tension component.

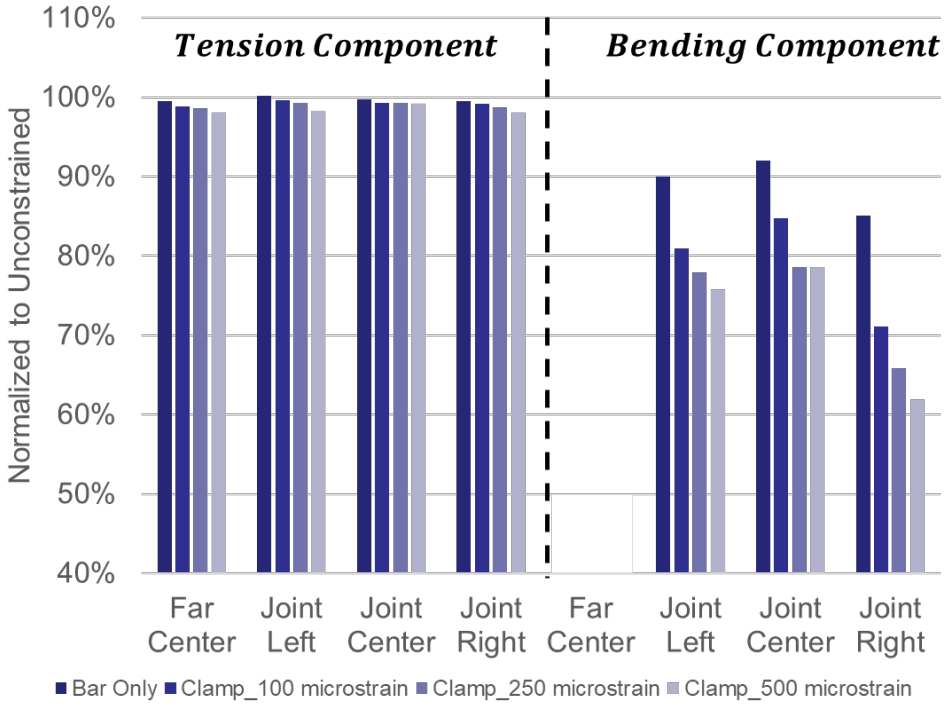

Figure 7: Anti-bend trial results.

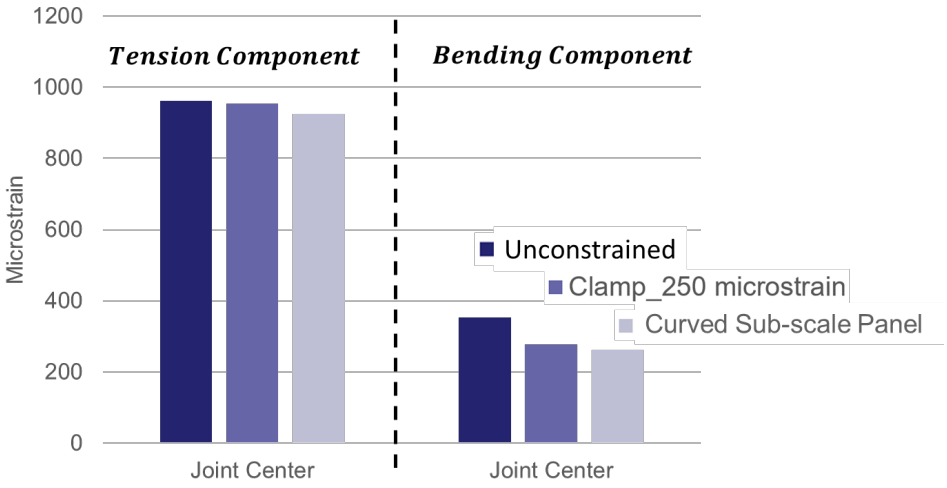

Figure 8: Anti-bend configuration selection

MSD Fatigue Crack Growth Results

To compare results across specimens, fatigue cycles are presented in this report as cycles after the lead crack reached a specific crack extension. This removes some of the variability in the notch sharpening phase and focuses the results on only the natural crack growth behavior. Reported fatigue cycles also include the underload cycles from the marker band spectrum. The marker bands were applied to all panels identically so their influence on fatigue cycle comparisons should be minimal.

At the beginning of each test, strain data was collected and compared to FEM results as well as previously completed panels. This information was used to validate the FEM and verify the loads are being applied to the panels correctly. A comparison of this data is shown in Figure 9. Due to the differences in loading mechanisms, the focus of the comparison is on the strain gages near the lap joint, particularly at the center of the panel near the lead crack. The strain gage data matched the FEA results reasonably well, especially considering the expected high strain gradients near the joint where the gages were installed.

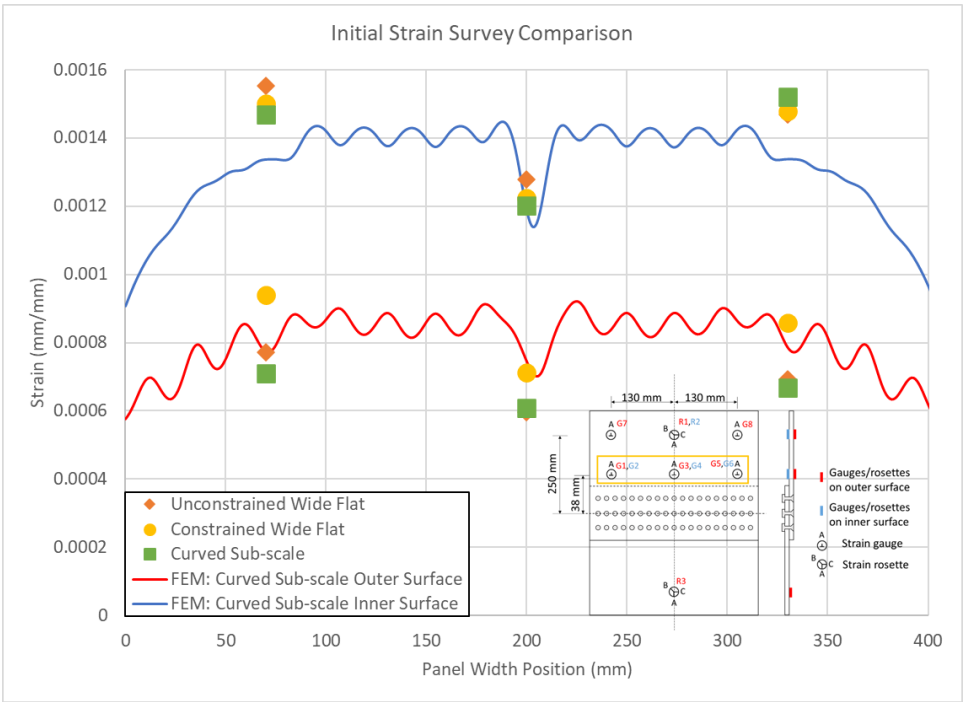

Figure 9: Strain gage comparison between FEM, wide flat panel, and curved sub-scale panel

As mentioned above, the fatigue tests were run until first crack link-up. For all tests, link-up occurred between the lead crack and adjacent MSD notch as expected. The purpose of the initial MSD scenario was to compare the crack growth behavior of the subject panels. As such, the fatigue cycles prior to the lead crack reaching an extension of 0.5 mm past the EDM notch were not included in the results. This removes the variability of the crack sharpening phase and gives a consistent starting point where natural cracks are growing. The fatigue results for the lead crack of each test are presented in Figure 10. Generally, the curved sub-scale panel lead cracks exhibited shorter fatigue life to first link-up compared to all the wide flat panels. The exception is curved sub-scale panel #2 which had the longest fatigue life of all tests. However, for curved sub-scale panel #2 the MSD notch adjacent to the lead crack was significantly slower, Figure 11, which contributed to the overall test length. The wide flat panels all had relatively similar lead crack growth regardless of the use of the anti-bend device. The device's effect was potentially only noticeable at the very end of the test where the constrained wide flat panels had a less severe jump in crack length.

A look at the lead crack growth rate for all the tests highlights the differences between the wide flat and curved sub-scale panels, as shown in Figure 12. The crack growth rates are calculated as an average rate between inspections, which were generally 2,000 cycles apart for the presented test data. From this perspective, it appears the curved sub-scale panels had a higher initial crack growth rate, then all panels had relatively the same rate in the middle phase, and finally the wide flat panels accelerated more rapidly at the end while the curved sub-scale panels maintained a steady increase. There is no distinguishable difference in crack growth rates between the wide flat panels in Figure 12 despite the use of the anti-bend device. This may be a result of the relatively large inspection intervals (2,000 cycles) that are used to calculate the crack growth rates. Recall from Figure 10 that the constrained wide flat panels did appear to show a less severe jump in lead crack length at the end of the test compared to the unconstrained ones. This end of test behavior did not show up in the crack growth rate comparison, so further analysis is being conducted via post-test fractography.

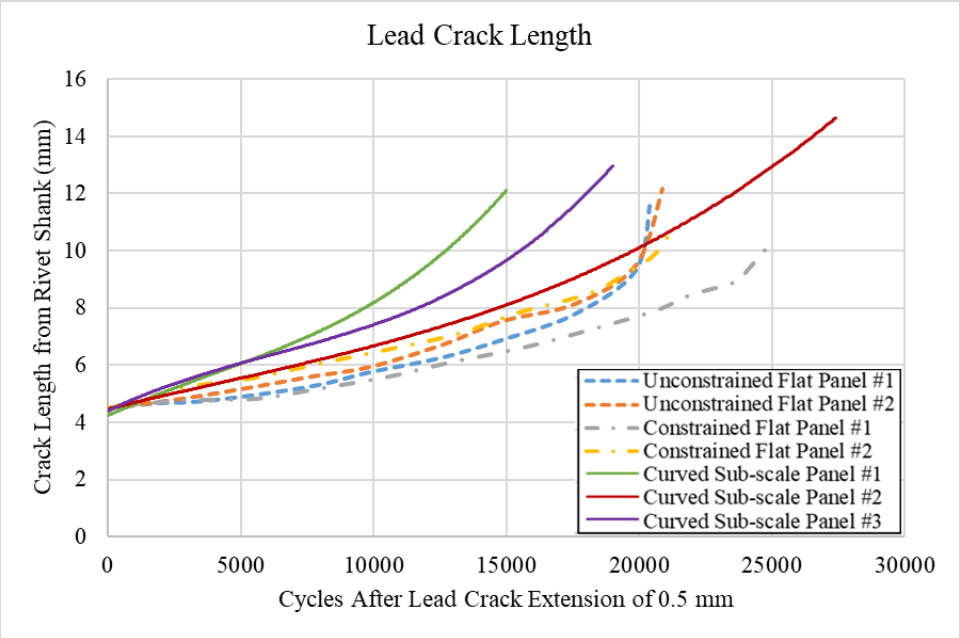

Figure 10: Lead crack length comparison

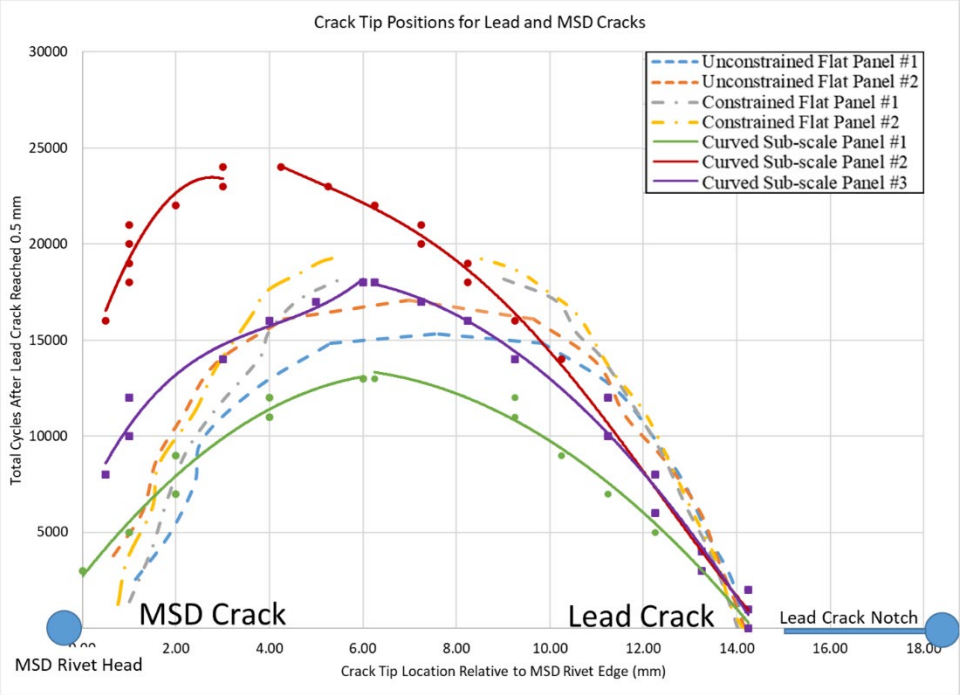

Figure 11: MSD crack length comparison

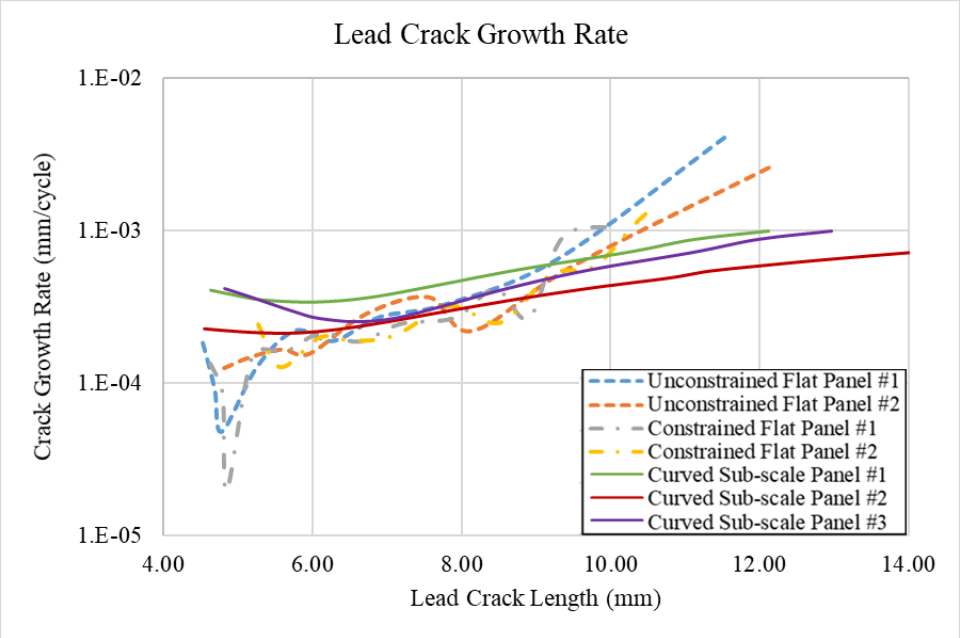

Figure 12: Fatigue crack growth rate comparison

Stress Intensity Factor Calculations

The two SIF calculation methods by DIC, based on the generalized Westergaard's equation and J-integral, were tested for one of the wide flat panels and compared to the FEM solution developed by Embraer. The results, shown in Table 1, represent good agreement between the three methods. Due to the nature of DIC, the two methods utilizing that data represent the estimated SIF at the surface. Accordingly, the FEM solution was calculated as near to the surface as possible. J-integral results calculated from the DIC data for the lead crack appear to be lower than expected, so more work is being done to understand if this is a result of the methodology or fidelity of the DIC results for this specific analyzed panel. All methods did have a good correlation for the secondary crack. Work is ongoing to apply these methodologies to all the panels tested.

Table 1: SIF solution comparison

SIF Method	Lead Crack (MPa*√mm)	Secondary Crack (MPa*√mm)
FEM	319	333
DIC (Westergaard)	302	333
DIC (J-integral)	260	303

Fractography

The inclusion of marker bands into the load history was done specifically to enable post-test fractography. The fatigue crack growth results presented previously were based on visual inspection for the wide flat panels and high frequency eddy current for the curved sub-scale panels. These methods are effective for real-time measurement during the test but may lack some accuracy and precision. The marker bands, however, leave a clear physical pattern on the fracture surface that indicates exactly where the crack front was at a certain inspection. An example of the output from fractography is shown in Figure 13. This is for the secondary crack of constrained flat panel #2. Here an SEM and post processing were used to collect and stitch together detailed images of the fracture surface. Marker bands are then located and mapped based on the specific pattern for the subject test specimen. A key thing to note is the curved crack front shape. The crack tunnels by growing faster at the faying surface due to the secondary bending which is an expected lap joint behavior. This means the surface inspections and SIF calculations presented in previous sections represent minimum values. Further, the second image in Figure 13 shows a comparison of the visual inspections, colored asterisks, to the mapped marker bands. While the visual inspections generally matched very well with their paired marker bands, there were some instances where they differed. While the marker bands make this fractography work much easier, it is still very time consuming. This work is still ongoing.

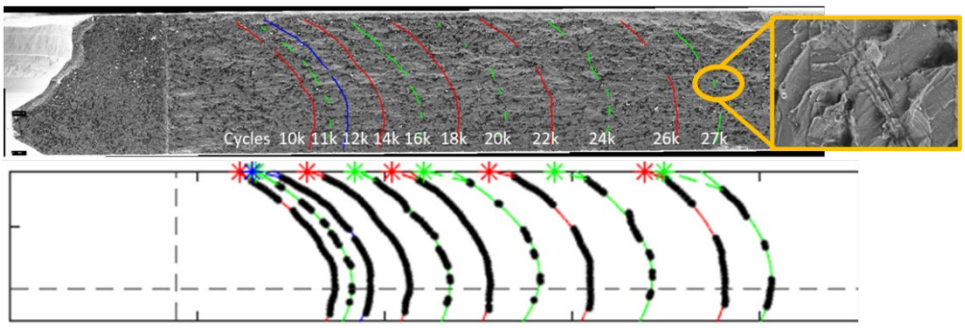

Figure 13: Marker band fractography analysis

SUMMARY

In a collaborative effort, the FAA, Arconic, Embraer, NIAR, and Drexel University are evaluating the behavior of multi-site damage (MSD) for emerging aluminum alloys in a generic fuselage lap joint configuration. This program is a comparative study of the initiation and growth characteristics of MSD for two aerospace aluminum alloys, namely: 2524-T3 aluminum-copper alloy (baseline) and 2060-T8 aluminum-lithium alloy (new generation). This paper specifically focuses on the efforts to study MSD growth from a common initial notch scenario for the 2524-T3 material only. A key focus of this work is evaluating coupon-scale effect using wide flat and curved sub-scale panel sizes. Substantial analytical and post-test fractography efforts are also being conducted to support the physical testing. Results and other major findings include:

- For this specific test matrix, the curved sub-scale panels generally exhibited a shorter fatigue life compared to all flat panels. Effects that may influence these results such as the secondary bending, stress biaxiality, and boundary conditions are being investigated
- Comparisons between curved sub-scale and wide flat panels can be considered in three phases

  - Initial crack growth where the curved sub-scale panels had higher crack growth rates
  - Stable crack growth where the curved sub-scale and flat panels showed similar crack growth rates
  - Final crack growth where the flat panel crack growth rates rapidly accelerated while the curved sub-scale panels remained relatively consistent
- An anti-bend device installed on a subset of wide flat panels had relatively little impact on the fatigue behavior
- SIF calculation methods using outputs from DIC matched reasonably well with FEM solutions for the wide flat panel example given
- Post-test fractography using marker bands was able to successfully map crack progression throughout the test

The program covered by this paper is still ongoing. Continued work is planned to apply the SIF methodologies and post-test fractography to the remaining wide flat and curved sub-scale panels. Additionally, further testing is planned to evaluate the influence of material selection and rivet installation on crack initiation and growth behaviors. Finally, the influence of the residual stresses from the roll forming manufacturing process on the curved sub-scale panel crack growth will be examined.

REFERENCES

[1] Kulak, M., Bakuckas, J. G., Tian, Y., Stanley, D. (2023). “Design, Analysis and Test Development of Full-Scale Fuselage Test Panels to Assess Emerging Metallic Structures Technologies,” [Unpublished manuscript], DOT/FAA/TC-TNxx/xx.

[2] Stonaker, K., Bakuckas, J., Stanley, D., Kulak, M., Chang, P., and Freisthler, M. (2019). “Assessment of Fatigue Behavior of Advanced Aluminum Alloys Under Complex Variable Amplitude Loading,” Proceedings of the 30th ICAF Symposium, June 5–7, 2019, Krakow, Poland.

[3] Tian, Y., Stanley, D. and Bakuckas, J. G., (2021). Assessment of Emerging Metallic Structures Technologies through Test and Analysis of Fuselage Structure: Test Panel 1. DOT/FAA/TC-21/25.

[4] Müller RPG. (1995), An experimental and analytical investigation on the fatigue behaviour of fuselage riveted lap joints. The significance of the rivet squeeze force, and a comparison of 2024-T3 and glare 3. Ph.D. thesis. The Netherlands: Delft University of Technology

[5] Fawaz, S. (2000). “Equivalent Initial Flaw Size Testing and Analysis,” AFRL-VA-WP-TR-2000-3024

[6] Skorupa, A. Skorupa, M. (2012), Riveted Lap Joints in Aircraft Fuselage; Design, Analysis and Properties, Springer, Dordrecht/Heidelberg/London/New York

[7] Dally, JW., Sanford, RJ. (1987), *Exp Mech*, vol 27, p. 381-8

[8] Ahmed, A., and Bakuckas, J. (2005). “Development of Multiple-Site Damage in Fuselage Structure,” DOT/FAA/AR-05/38

[9] Stanley, D., Awerbuch, J., Tan, T., Anasori, B. (2016), *Theoretical and Applied Fracture Mechanics*, vol 82, p. 33-50